ADAPTING THE SIR ALGORITHM TO ASCAT

Richard D. Lindsley and David G. Long

Brigham Young University, MERS Laboratory, 459 CB, Provo, UT 84602

1. INTRODUCTION

The ESA/EUMETSAT ASCAT (Advanced SCATterometer) is one of the latest remote sensing instruments in Earth orbit. ASCAT is a C-band scatterometer deployed on the MetOp-A platform. Although it is designed to measure wind fields over the oceans, the radar backscatter over land and ice is collected and is useful in land and ice studies.

The SIR (Scatterometer Image Reconstruction) algorithm [1, 2] has been successfully used for other scatterometers. We apply the SIR algorithm to ASCAT for two reasons: to extend the C-band scatterometer land and ice time series (last updated by ERS) and to compare with Ku-band scatterometer data, including QuikSCAT.

SIR enhances the resolution of scatterometer data by combining data from overlapping measurements over the same region. Over a range of incidence angles θ_i, measurements of radar backscatter σ^0 can be modeled as

$$10 \log_{10} \sigma^0 = \mathcal{A} + (\theta_i - 40^\circ)\mathcal{B} \tag{1}$$

where $\mathcal{A}$ and $\mathcal{B}$ are functions of polarization, azimuth angle, and physical characteristics of the region corresponding to the σ^0 measurement. $\mathcal{A}$ is in dB and represents the σ^0 value normalized to a 40° incidence angle. $\mathcal{B}$ is in dB/° and describes the dependence of σ^0 on θ_i [1, 2, 3, 4].

ASCAT data as processed by EUMETSAT come in three products: SZO, SZR, and SZF. The SZO and SZR products contain spatially-averaged σ^0 measurements. 50 km resolution SZO data is not considered in this paper. 25 km resolution SZR data is comparable to QuikSCAT 'eggs,' and the full resolution SZF data is comparable to QuikSCAT 'slices.'

This paper details how we adapt the SIR algorithm to work with ASCAT. We first use both SZR and SZF ASCAT data with SIR to generate enhanced resolution imagery. Finally, we tune the SIR parameters for ASCAT.

2. USING SIR ON ASCAT DATA

Because of its similarity to previous scatterometers, much of the effort in applying the SIR algorithm to ASCAT SZR data has been previously done with the ERS scatterometer. We reuse the ERS point-response function and scale it

by half to fit the 25 km grid used by ASCAT SZR data.

Applying the SIR algorithm to the SZF data requires some more attention. We present some background to the data format and illustrate our method to approximate the σ^0 spatial response.

2.1. Background

The ASCAT SZF files are organized such that each measurement and its associated data are grouped into a 'node.' Each node contains several values needed for the SIR algorithm, except for the spatial response function of each σ^0 measurement. Unfortunately, detailed information on individual ASCAT σ^0 measurement spatial response functions is limited.

Ideally, a full 3D response function for each node would be used. Instead, we use a binary approximation of the main lobe, where the approximate response is set to 1 from the response center to where the two-way response drops off 6 dB, and 0 elsewhere (this ignores any contributions of the side lobes to σ^0). This approximation traces out a two-dimensional ellipsoidal-like binary mask and is roughly equivalent to the spatial extent of a node. A similar approach is used on QuikSCAT slices.

Without knowing the precise shape of the ellipsoidal mask, we approximate it by determining a rectangular area that is equivalent to the true spatial extent. We term the rectangular area for each node a 'slice,' echoing the terminology used for QuikSCAT. Because the slice is rectangular, the area bounded by each slice is characterized by the location of the four corners of the slice.

2.2. Method

Each node n (except the first and last nodes in a beam) is bordered on either side by another node. To find the slice boundaries for a node n, the slice width is determined by using the midpoint between a node and its two adjacent nodes. This is indicated in Fig. 1 by the two X marks. The slice length d is determined by using the 3-dB azimuthal beamwidth of the antenna (θ) and the slant range ρ_d to node n in the relation $d = \rho_d \cdot \theta$. We make an additional approximation here that the sides of the slice are perpendicular to the along-beam direction.

This method for calculating the shapes for each slice is incorporated into the ASCAT SZF SIR code. We note that although there are several approximations involved in this process, the SIR images are relatively insensitive to reasonable changes in these values. Changing the values affects the final image only slightly.

3. TUNING SIR PARAMETERS

The SIR algorithm has four parameters that are tuned for each instrument it is applied to: the number of iterations (N_{its}) of SIR, the $\mathcal{A}$ and $\mathcal{B}$ initialization values (A_{init} and B_{init}), and $\mathcal{B}$-value weighting.

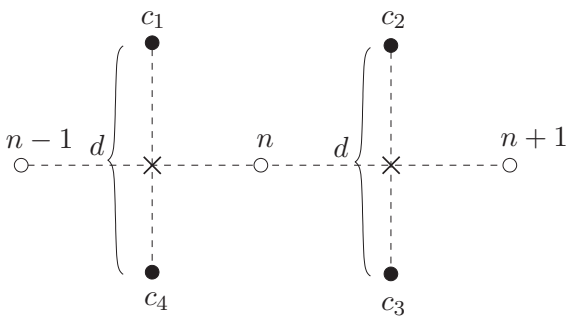

Fig. 1. Slice geometries. Empty circles are node positions for consecutive nodes. Node midpoints are marked with an X. Slice corners are indicated by the filled black circles. The width of a slice is determined by midpoints to neighboring nodes, and the length of a slice is determined by d, as explained in the text.

To find optimum SIR parameter values, we start with default values from ERS and follow a procedure based on previous SIR parameter tunings [3, 4]: using a series of truth images, Monte Carlo simulated measurements are synthetically created from the true image using the geometry of an actual pass. SIR is performed on the simulated measurements for a variety of different SIR parameter values. Using various metrics, we compare SIR outputs with the truth images and choose SIR parameter values that lead to the overall best metric values.

The first SIR parameters to be determined are N_{its} and B_{weight}. We run the SIR algorithm on the simulated measurements using a constant-value truth image. After each SIR iteration, the mean and standard deviation are calculated for the difference between the truth image and the SIR output. From comparing the results, we choose $N_{\text{its}} = 35$ for SZF data, and $N_{\text{its}} = 27$ for SZR data. We also find $B_{\text{weight}} = 50$ suitable for ASCAT for both SZR and SZF data.

Different values for A_{init} and B_{init} are tested using a non-constant truth image to simulate rivers and other land features [4]. We use four metrics to analyze the results: mean error, standard deviation, RMS error, and the correlation coefficient. We conclude that the $\mathcal{A}$ and $\mathcal{B}$ initialization values should be set to $A_{\text{init}} = -15$ and $B_{\text{init}} = -0.25$.

Figure 3 shows zoomed portions of $\mathcal{A}$ SIR images processed using ASCAT data for a 24-hour period in Antarctica, and for a four-day period in North America. The SZF data yield higher resolution images than SZR data.

4. PRELIMINARY ASCAT SIR ANALYSIS

In this paper, we assume that the σ^0 value for a surface is the same regardless of the azimuth direction from ASCAT. This assumption is valid for many areas of interest on the Earth, but does not hold over eastern Antarctica. This is an

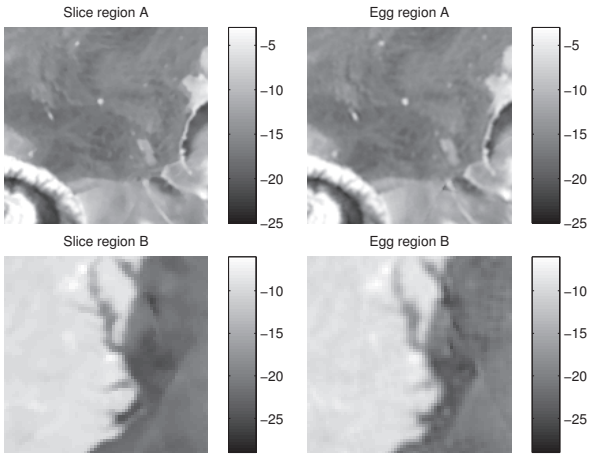

Fig. 2. The top row is a comparison of a region of Antarctica (JD 214 2008) using SZF (slice) and SZR (egg) data. The bottom row similarly shows a section of the coast of North Carolina (JD 257–260 2009).

effect documented previously for ERS and QuikSCAT [5, 6]. We will account for σ^0 azimuth variations for ASCAT in subsequent work.

In comparing SIR images for both ASCAT and QuikSCAT, we note that the σ^0 variance over ocean is greater for QuikSCAT than for ASCAT. Also, σ^0 variance over land is greater for ASCAT than for QuikSCAT. This difference can be exploited to aid in sea ice detection and estimation.

5. REFERENCES

[1] D. S. Early and D. G. Long, "Image Reconstruction and Enhanced Resolution Imaging from Irregular Samples," *IEEE Transactions on Geoscience and Remote Sensing*, vol. 39, no. 2, pp. 291–302, 2001.

[2] D. G. Long, P. Hardin, and P. Whiting, "Resolution Enhancement of Spaceborne Scatterometer Data," *IEEE Transactions on Geoscience and Remote Sensing*, vol. 31, pp. 700–715, 1993.

[3] Q. P. Remund, "Refinement of SIRF for SASS," Tech. Rep., BYU MERS Technical Report #98-04, 1998.

[4] Q. P. Remund and D. G. Long, "Optimization of SIRF for NSCAT," Tech. Rep., BYU MERS Technical Report #97-03, 1997.

[5] D. S. Early and D. G. Long, "Azimuth Modulation of C-band Scatterometer Sigma-0 Over Southern Ocean Sea Ice," *IEEE Transactions on Geoscience and Remote Sensing*, vol. 35, no. 5, pp. 1201–1209, 1997.

[6] Q. P. Remund, D. S. Early, and D. G. Long, "Azimuth Modulation of Ku-band Scatterometer Sigma-0 over the Antarctic," Tech. Rep., BYU MERS Technical Report #97-02, 1997.